

Tuning the interactions in the spin-ice materials $\text{Dy}_2\text{Ge}_{2-x}\text{Si}_x\text{O}_7$ by silicon substitution

T. Stöter,^{1,2} M. Antlauf,³ L. Opherden,^{1,2} T. Gottschall,² J. Hornung,^{1,2} J. Gronemann,^{1,2} T. Herrmannsdörfer,² S. Granovsky,^{1,4} M. Schwarz,³ M. Doerr,¹ H.-H. Klauss,¹ E. Kroke,³ and J. Wosnitza^{1,2}

¹*Institut für Festkörper- und Materialphysik, TU Dresden, 01062 Dresden, Germany*

²*Dresden High Magnetic Field Laboratory (HLD-EMFL),*

Helmholtz-Zentrum Dresden-Rossendorf, 01328 Dresden, Germany

³*Institut für Anorganische Chemie, TU Bergakademie Freiberg, 09596 Freiberg, Germany*

⁴*Faculty of Physics, M. V. Lomonosov Moscow State University, 119991 Moscow, Russia*

(Dated: August 9, 2019)

We report that the lattice constant of $\text{Dy}_2\text{Ge}_{2-x}\text{Si}_x\text{O}_7$ ($x = 0, 0.02, 0.08, 0.125$) can be systematically reduced by substituting the non-magnetic germanium ion in the cubic pyrochlore oxide with silicon. A multi-anvil high-pressure synthesis was performed up to 16 GPa and 1100 °C to obtain polycrystalline samples in a solid-state reaction. Measurements of magnetization, ac susceptibility, and heat capacity reveal the typical signatures of a spin-ice phase. From the temperature shift of the peaks, observed in the temperature-dependent heat capacity, we deduce an increase of the strength of the exchange interaction. In conclusion, the reduced lattice constant leads to a changed ratio of the competing exchange and dipolar interaction. This puts the new spin-ice compounds closer towards the phase boundary of short-range spin-ice arrangement and antiferromagnetic long-range order consistent with an observed reduction of the energy scale of monopole excitations.

PACS numbers: 75.40.Cx, 75.40.Gb, 81.10.-h

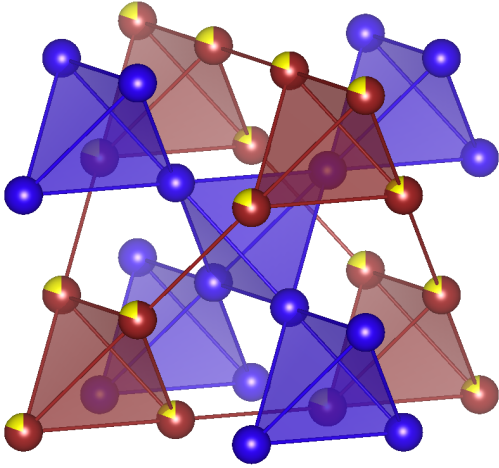


FIG. 1. Structure of $\text{Dy}_2\text{Ge}_{2-x}\text{Si}_x\text{O}_7$: the A site is occupied by Dy^{3+} (shown as blue spheres) and the B site is partially occupied by Si^{4+} and Ge^{4+} shown as red spheres with a yellow segment; the oxygen atoms are omitted.

I. INTRODUCTION

Magnetically frustrated materials have attracted considerable interest because of their rich magnetic phases hosting exotic states of matter and emergent excitations^{1,2}. Frustration in a magnetic material can lead to a ground-state manifold without long-range order¹. This can occur in various possible ways, such as via antiferromagnetic (AFM) nearest-neighbor coupling of Ising spins on a triangular lattice or a periodical variation of magnetic interactions between nearest neighbors^{3,4}.

In the case of pyrochlore oxides $A_2B_2O_7$ with a trivalent ion A^{3+} and a tetravalent ion B^{4+} (Fig. 1), frustration can arise due to the strong crystal electric field acting on the ions on the pyrochlore lattice of corner-sharing tetrahedra. For pyrochlores with a rare-earth ion on the A site many different exotic states have been observed, such as classical or quantum spin-ice states with magnetic-monopole excitation^{2,5-9}. Specifically, for the pyrochlores with Dy and Ho on the A site, the rare-earth ion is subject to a strong crystal-electric-field splitting of the ground state and the first excited state of the single ion by an energy of the order of 200 K¹⁰. The single-ion ground state is an effective spin-half state¹¹ pointing either in or out of the tetrahedra the ion belongs to. The two-ion interaction is well described by the dipolar spin-ice model which includes dipolar D_{nn} and exchange interaction J_{nn} to form an effective interaction $J_{\text{eff}} = D_{nn} + J_{nn}$ between nearest neighbors¹². Following this simple spin-ice model¹² for $\text{Ho}_2\text{Ti}_2\text{O}_7$ and $\text{Dy}_2\text{Ti}_2\text{O}_7$, the competing interactions result in an effective ferromagnetic nearest-neighbor interaction $J_{\text{eff}} > 0$, and a positioning of these compounds on the right-hand side of the phase diagram of this model Fig. 2 – in contrast, neodymium-based pyrochlores (*e.g.* $\text{Nd}_2\text{Zr}_2\text{O}_7$) adopt an AFM long-range ordered phase situated on the left-hand side of Fig. 2¹³⁻¹⁶ because of a different relation of exchange to dipolar interaction. An effective interaction $J_{\text{eff}} > 0$ favors the highly degenerate spin-ice configuration: two spins point into and two spins point out of each tetrahedron (“2-in-2-out”)¹⁷. The excitations of this arrangement can be interpreted as the creation of magnetic monopole-antimonopole pairs¹⁸. In several investigations of $\text{Dy}_2\text{Ti}_2\text{O}_7$ and $\text{Ho}_2\text{Ti}_2\text{O}_7$ via ac-susceptibility measurements¹⁹⁻²⁸ thermally-activated spin dynamics have been found that are attributed to the thermal exci-

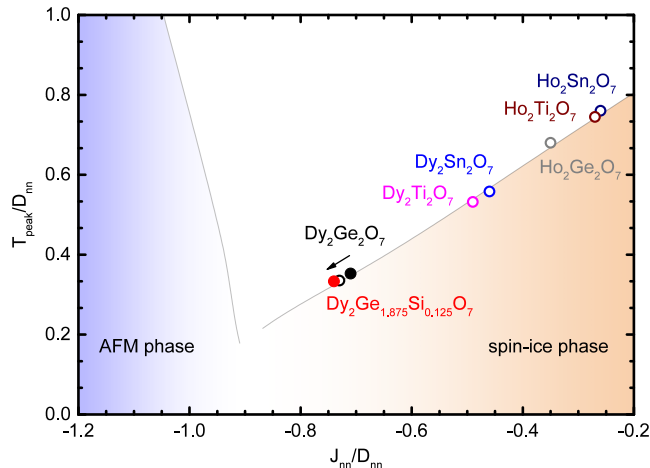


FIG. 2. Phase diagram of the dipolar spin-ice model¹² including the positions of several spin-ice compounds and the phase boundaries of the antiferromagnetic (AFM) and the spin-ice phase. Data from literature³⁸ are shown as open circles, filled symbols stand for the samples from this work. J_{nn} and D_{nn} denote the exchange and dipolar interaction between nearest neighbors, respectively. T_{peak} denotes the temperature of the peak in the heat capacity associated with the spin-ice phase (adapted from Zhou *et al.*³⁸).

tation of monopoles²⁹. The magnetization and specific-heat measurements of the spin-ices show characteristic behavior like a liquid-gas transition at sub-kelvin temperatures in field-dependent measurements^{30–32} or a Schottky-like anomaly in temperature-dependent measurements at zero field^{33–35}, respectively. A strong experimental evidence for the dipolar spin-ice character is the residual Pauling entropy of $S = 1/2 \ln(3/2)R$ calculated from measurements of the specific heat^{12,36,37}.

Although recent publications^{37,39} discuss deviations from this Pauling’s ice-rule entropy due to extremely slow relaxation dynamics below 1 K, a non-vanishing entropy on shorter time scales remains a prerequisite of the spin-ice state³⁷. Theoretical investigations of spin-ice models including interactions beyond nearest neighbors find a long-range ordered ground state satisfying the ice-rules^{40–45}. Comparing our samples with these refined models lies beyond our experimental possibilities and we concentrate on the dependence of the nearest-neighbor exchange constant J_{eff} on the Si substitution x in $\text{Dy}_2\text{Ge}_{2-x}\text{Si}_x\text{O}_7$.

Especially in the vicinity of the transition between long-range (AFM) and short-range (spin-ice) correlations, new magnetic states may occur^{46,47}. Therefore, tuning the internal interactions seems a promising route to investigate these new states within this domain of the phase space. Instead of the experimentally difficult application of hydrostatic pressure to existing sample that manipulates the nearest-neighbor distance⁴⁸, the interaction between neighboring rare-earth ions can be var-

ied by exchanging the B site ion with one of different ionic radius^{38,47}. For example, substituting Ge for Ti in $\text{Dy}_2\text{Ti}_2\text{O}_7$ reduces the distance between the Dy ions and thus changing the relative strengths of the competing dipolar and exchange interactions, D_{nn} and J_{nn} , respectively³⁸. The total effective interaction J_{eff} is reduced shifting the compound closer to the not yet experimentally investigated phase region just between the spin-ice and AFM phase in the dipolar spin-ice model, see Fig. 2.

The next challenge is to synthesize a material with an even smaller B site ion than Ge, such as Si, allowing for further tuning the balance of exchange (J_{nn}) and dipolar interactions (D_{nn}) in a spin-ice compound. This new ratio J_{nn}/D_{nn} allows for investigating pyrochlores closer to the crossover region between frustration-driven dynamics and magnetic order than ever before.

But many combinations of A and B site ions have an unstable pyrochlore phase when synthesized at ambient pressure⁴⁹. Mouta *et al.*⁴⁹ have empirically investigated the stability of the pyrochlore structure with respect to the ratio of the atomic radii r_a/r_b , where r_a and r_b denote the atomic radii of the A site and B site ions, respectively. At ambient pressure, stable pyrochlores can be realized for ratios $1.36 < r_a/r_b < 1.71$ ^{8,47}. For comparison, the ratio of the ionic radii for Dy^{3+} on the A site and Ti^{4+} , Ge^{4+} , and Si^{4+} on the B site are 1.70, 1.94, and 2.57, respectively. Under high hydrostatic pressure during synthesis, the stability range can be extended towards smaller r_b , e.g. from $\text{Dy}_2\text{Ti}_2\text{O}_7$ to $\text{Dy}_2\text{Ge}_2\text{O}_7$. The resulting pyrochlores persist metastable also under ambient pressure conditions⁴⁷.

While for the growth of $\text{Dy}_2\text{Si}_2\text{O}_7$ with the hypothetical ratio $r_a/r_b = 2.57$, pressures beyond the state of the art would be needed or this phase would be inherently unstable, we were able to grow stable $\text{Dy}_2\text{Ge}_{2-x}\text{Si}_x\text{O}_7$ polycrystals with Si substitution of up to $x = 0.125$ under high-pressure and high-temperature conditions. In this paper, we show that such a substituted compound exhibits the characteristic properties of a classical spin-ice material while having reduced effective interactions that shift its magnetic state further towards the phase boundary between spin-ice and AFM order.

II. EXPERIMENTAL

Polycrystalline Dy germanate $\text{Dy}_2\text{Ge}_2\text{O}_7$ was synthesized similar as described previously^{46,50}: GeO_2 (Heraeus, 99.999%) and Dy_2O_3 (Chempur, 99.999%) were used as starting materials. Stoichiometric amounts were mixed with ethanol and thoroughly ground in an agate mortar until dryness. The synthesis was performed in a “Walker-type” high-pressure apparatus⁵¹ with a 1000 t hydraulic press (Voggenreiter GmbH). The powder mixture was filled in an h -BN capsule and compressed in an 18 mm zirconia octahedron pressure medium with a load of 970 t corresponding to a sample pressure of 8 GPa.

The pyrochlore material forms during a solid-state reaction at 1100 °C maintained for 90 min. The temperature was measured with a Type C (W5%Re/W26%Re) thermocouple.

For the polycrystalline silicone-substituted $\text{Dy}_2\text{Ge}_{2-x}\text{Si}_x\text{O}_7$ samples, SiO_2 (Degussa Aerosil380, > 99.8%) was used additionally. The uni-axially pre-pressed samples were surrounded by CsCl capsules and compressed in 10 mm MgO:Cr octahedral pressure cells (Ceramic Substrate & Components Ltd.) with a load of 642 t which equals a sample pressure of approximately 16 GPa. Si-containing pyrochlores were synthesized at 1100 °C for 90 to 180 min. We recovered polycrystalline, sintered pieces of dark to light gray material after the high-pressure synthesis of $\text{Dy}_2\text{Ge}_{2-x}\text{Si}_x\text{O}_7$ with $x = 0, 0.02, 0.08$, and 0.125. The phase purity was confirmed via SEM/EDX analysis (Carl Zeiss LEO 1530) for all samples and via room-temperature x-ray powder diffraction at the ALBA synchrotron light source (Beamline 4, $\lambda = 0.413364 \text{ \AA}$) in Barcelona, Spain, for $\text{Dy}_2\text{Ge}_2\text{O}_7$ and by using a Seifert diffractometer (FPM URD6) in symmetric Bragg-Brentano-Geometry with Cu anode for $\text{Dy}_2\text{Ge}_{2-x}\text{Si}_x\text{O}_7$ with $x = 0.02, 0.08$, and 0.125. The software package Fullprof (Suite 3.00, 2015) was used for the Rietveld analysis to obtain the lattice constants.

Magnetization measurements were performed using a commercial SQUID magnetometer (MPMS) and a vibrating-sample magnetometer in magnetic fields up to 7 T. Magnetic ac-susceptibility measurements were performed in a compensated coil-pair susceptometer at frequencies ranging from 4 to 1293 Hz down to a temperature of 0.3 K using a commercial ^3He system. The temperature was measured with a RuO_2 resistance thermometer. Demagnetization effects²⁸ were estimated and found to be of no importance for our arguments. The heat capacity of $\text{Dy}_2\text{Ge}_2\text{O}_7$ and $\text{Dy}_2\text{Ge}_{1.875}\text{Si}_{0.125}\text{O}_7$ was measured using the quasi-adiabatic heat-pulse method⁵² in which the sample is heated by a short pulse of defined energy while the resulting temperature change is measured. For this the sample is placed on a sapphire platform in a ^3He sorb-pumped cryostat with a carefully calibrated RuO_2 thermometer.

III. RESULTS AND DISCUSSION

The diffraction data of unsubstituted Dy germanate confirmed the cubic pyrochlore structure ($Fd\bar{3}m$, 227) with a lattice constant of $a = 9.930(1) \text{ \AA}$, which is in excellent agreement with the literature data ($a = 9.929 \text{ \AA}$ ⁴⁶). Rietveld refinements show that the pyrochlore structure can well describe the diffraction patterns of $\text{Dy}_2\text{Ge}_{1.98}\text{Si}_{0.02}\text{O}_7$, $\text{Dy}_2\text{Ge}_{1.92}\text{Si}_{0.08}\text{O}_7$, and $\text{Dy}_2\text{Ge}_{1.875}\text{Si}_{0.125}\text{O}_7$ (the latter is shown in Fig. 3) with lattice constants $a = 9.924(1) \text{ \AA}$, $9.912(1) \text{ \AA}$, and $9.906(1) \text{ \AA}$, respectively. We achieved the best fit by assuming a statistical substitution of Ge with Si on the B

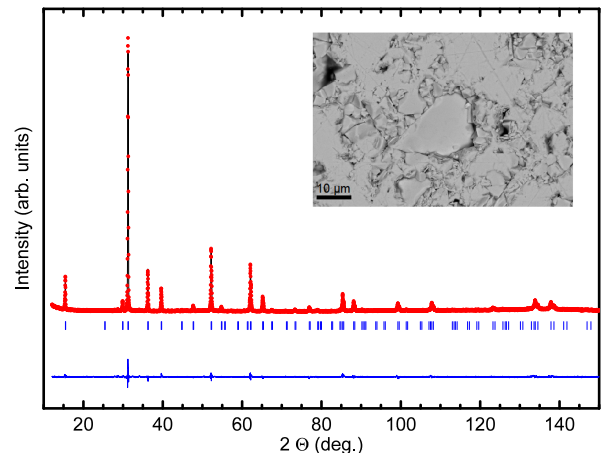


FIG. 3. Powder-diffraction pattern and Rietveld-difference plot for $\text{Dy}_2\text{Ge}_{2-x}\text{Si}_x\text{O}_7$ with $x = 0.125$, fitted for this stoichiometry. Inset: SEM micrograph of the polished sample surface, revealing crystallite sizes up to approximately 15 μm .

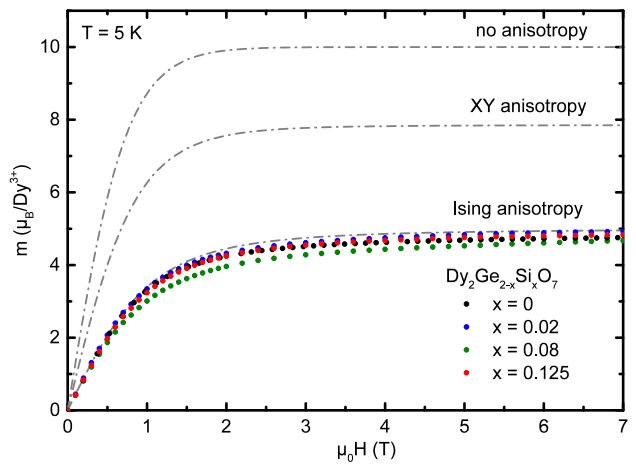


FIG. 4. Field dependence of the magnetization per dysprosium ion of $\text{Dy}_2\text{Ge}_{2-x}\text{Si}_x\text{O}_7$ with $x = 0, 0.02, 0.08$, and 0.125 at a temperature of 5 K. The symbols are measured values and the dash-dotted lines correspond to the powder-averaged Boltzmann distribution of spin-half spins with Ising-anisotropy, XY-anisotropy, and with no anisotropy, respectively. The error bars are within the size of the symbols.

site of the pyrochlore structure with exactly the Si concentration of the starting-material mixtures. In particular, Si is not interstitially incorporated into the crystal. There were no signs for chemical inhomogeneities or additional phases in XRD or SEM investigations (Fig. 3).

In Fig. 4, the magnetization per Dy ion of the sample series is shown as a function of magnetic field measured at low temperatures and consistent with the literature⁵³. The field dependence of the magnetization is well de-

scribed by a powder-averaged Boltzmann distribution of non-interacting paramagnetic Ising spins (dash-dotted curve) resulting in a magnetic moment of $4.80(15)\mu_B$ per Dy at saturation while the Heisenberg model (no anisotropy) or the case of XY-anisotropy would result in a very different magnetic behavior. It should be noted that the magnetization values at the maximum field do not systematically depend on the Si concentration. The deviations can be attributed to the use of polycrystalline samples which, due to the growing process, may contain a degree of texture which is not visible in the diffractograms. However, the low scattering of the measuring points shows the accuracy of the magnetization measurements. For the calculation of the D_{nn} the value of $10\mu_B$ for the free moment was used. The Curie-Weiss temperature θ_{CW} of our $Dy_2Ge_2O_7$ sample is close to zero and consistent with the literature value³⁸; the difference of θ_{CW} of the Si containing samples compared to $Dy_2Ge_2O_7$ is within the accuracy of the measurement of approximately ± 0.5 K.

To detect distinct differences, we will focus our investigation for the remainder of this article on pure Dy germanate and the sample with the highest Si substitution, $Dy_2Ge_{1.875}Si_{0.125}O_7$. Figure 5(a) shows the real (χ') and imaginary part (χ'') of the ac susceptibility of the substituted and unsubstituted sample for three exemplary frequencies. The distinct frequency dependence is visible especially in χ'' . Both samples show sharp maxima which shift towards higher temperatures and smear out continuously at higher frequencies. At 16 Hz, $Dy_2Ge_{1.875}Si_{0.125}O_7$ has a peak temperature of 580 mK being about 50 mK lower than for $Dy_2Ge_2O_7$. Furthermore, it is observed that the increase of the peak temperature at higher frequencies is much less pronounced in the substituted compound. Demagnetization effects should not influence our following qualitative discussion, even though they can cause deviations of the measured susceptibility, for the absolute values as well as for the peak positions^{23,28}. They should cause similar changes for the equally shaped $Dy_2Ge_2O_7$ and $Dy_2Ge_{1.875}Si_{0.125}O_7$ samples; however, an analytical determination of the demagnetization factor for our disc-shaped samples is not possible.

Based on the ac-susceptibility results, the spin dynamics can be investigated further. At the peak temperature T_P of the imaginary part χ'' at a given attempt frequency f , the spin-relaxation time τ is related to f via $\tau = 1/2\pi f$. In Fig. 5(b), the spin-relaxation time is plotted vs. the inverse of the temperature T_P . $Dy_2Ge_2O_7$ has two linear regions; a high-temperature region above about 0.8 K that is less steep than the low-temperature region. In $Dy_2Ge_{1.875}Si_{0.125}O_7$ only one slope is found below 1 K. We focus our discussion on the low temperature region. At low measurement frequencies, the relaxation times seem to follow an Arrhenius law (dashed lines in Fig. 5(b)):

$$\tau(T_P) = \tau_0 \exp(\Delta/k_B T_P). \quad (1)$$

The energy barriers Δ used to fit the data change only little, from 6.8(2) K to 6.70(5) K, due to the partial substitution of Ge by Si. Instead, the shift of the peak positions of χ'' from $Dy_2Ge_2O_7$ to $Dy_2Ge_{1.875}Si_{0.125}O_7$ mainly result in a change of the pre-exponential factor τ_0 from 250(50) ns to 90(10) ns due to the Si substitution. This pre-exponential factor is attributed to the spin-tunneling rate between the two Ising states and should be determined by the systems CEF level scheme and the transverse fields acting on the flipping spin^{29,54}. The reduction of τ_0 with substitution of Ge by Si is not surprising, as it decreases also with decreasing lattice constant from $Dy_2Sn_2O_7$ to $Dy_2Ti_2O_7$ ⁵⁵. Due to the similar shape of the samples, demagnetization effects are unlikely to alter the qualitative observation of a reduction of the pre-exponential factor from $Dy_2Ge_2O_7$ to $Dy_2Ge_{1.875}Si_{0.125}O_7$.

Apart from the influence of the mere lattice contraction, however, the random distribution of Si and Ge on the B site may contribute to this reduction. Possibly, the lowering of the local site symmetry influences the Ising character of the single ion inducing transverse exchange coupling¹¹ as perturbation of the dominant Ising interaction. Such transverse exchange coupling might reduce τ_0 as proposed in other rare-earth compounds with spin-ice character⁵⁶.

The magnetic specific heat c_{mag} of $Dy_2Ge_2O_7$ and $Dy_2Ge_{1.875}Si_{0.125}O_7$ in external fields up to 4 T is shown in Fig. 6. The unsubstituted sample has a peak in the heat capacity at a temperature of 0.84(1) K, determined by a phenomenological fit, whereas the substituted compound has a slightly reduced peak position of 0.80(1) K and an increased peak height. Since this work deals with polycrystalline samples, as does Ref.³⁸, the peak height can be influenced by factors both in production and measurement. However, a rise of the peak height in the substituted sample fits into the picture of a smaller J_{nn}/D_{nn} ¹².

This Schottky-like peak is associated to spin-freezing and establishment of the spin-ice state³⁶. Even though the peak temperature is shifted only by a small amount, it is a strong hint that the substitution of Si leads to a shift towards the boundary between spin-ice and AFM phase in the phase diagram (Fig. 2). At temperatures above the peak position, both compounds show almost the same specific heat; above 10 K the phononic contribution becomes dominant. Measurements up to 30 K are used to determine this contribution in order to extrapolate it to the low-temperature specific heat. The magnetic specific heat is the total specific heat minus the phononic contribution. The feature in the specific heat of $Dy_2Ge_{1.875}Si_{0.125}O_7$ at about 3 K could indicate the possible presence of a minority phase that was not visible in the XRD studies. Furthermore, a broadening of the specific-heat peak of the substituted material towards lower temperatures compared to $Dy_2Ge_2O_7$ can be seen. However, in an ideal spin-ice with smaller J_{nn}/D_{nn} than $Dy_2Ge_2O_7$ we would rather expect a narrowing of

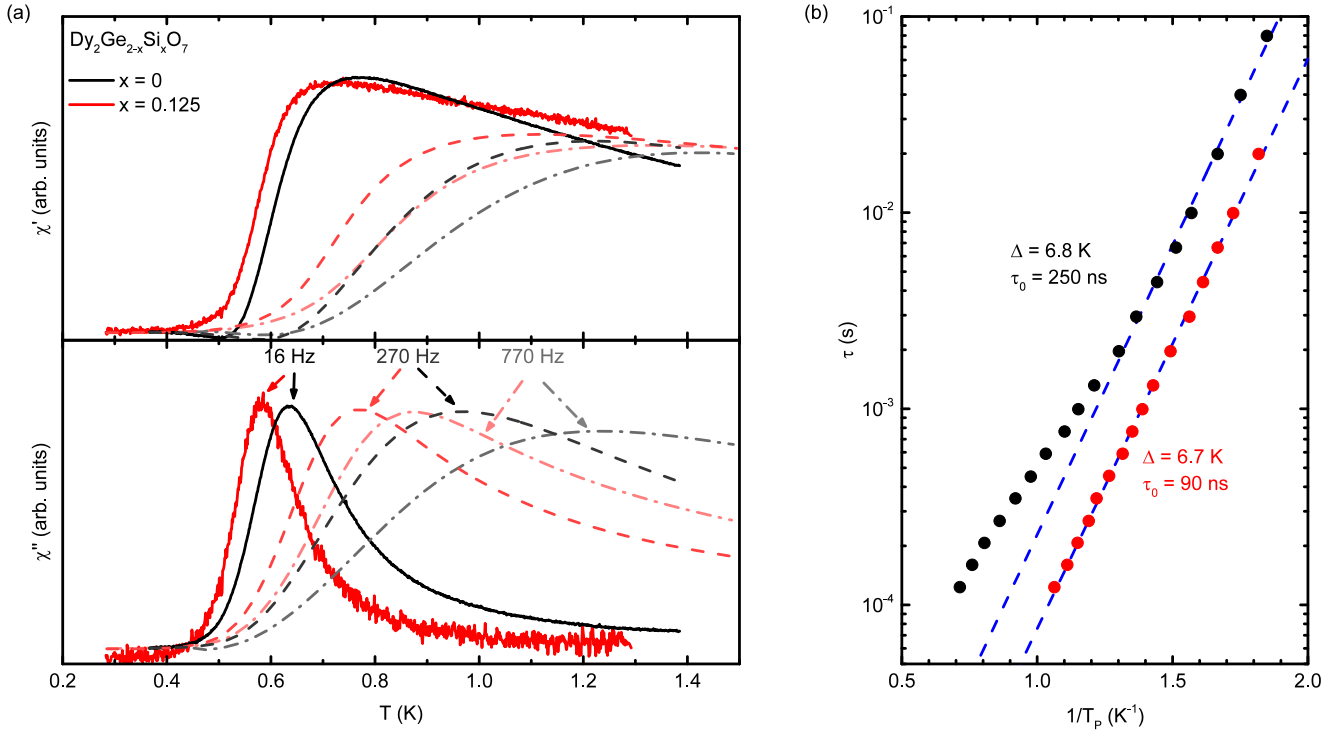


FIG. 5. (a) Real and imaginary part of the ac susceptibility χ' and χ'' of $\text{Dy}_2\text{Ge}_2\text{O}_7$ (black) and $\text{Dy}_2\text{Ge}_{1.875}\text{Si}_{0.125}\text{O}_7$ (red) at frequencies of 16 (solid), 270 (dashed), and 770 Hz (dash-dotted). (b) Spin-relaxation time $\tau = (2\pi f)^{-1}$ as a function of the inverse peak temperature T_P . Fits using the Arrhenius law with their respective energy barriers Δ are shown as dashed lines. The data are not corrected for demagnetization.

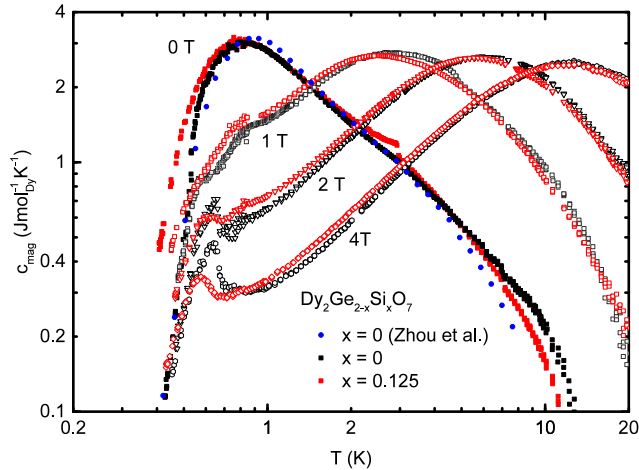


FIG. 6. Temperature dependence of the magnetic specific heat c_{mag} per mole Dy of the $\text{Dy}_2\text{Ge}_2\text{O}_7$ and $\text{Dy}_2\text{Ge}_{1.875}\text{Si}_{0.125}\text{O}_7$ samples in black and red symbols, respectively. The zero-field data is marked by full symbols and the data at 1, 2 and 4 T by empty symbols. Specific heat data for $\text{Dy}_2\text{Ge}_2\text{O}_7$ from Zhou *et al.*³⁸ (blue) have been included for comparison.

the specific-heat peak¹². The origin for this broadening could be related to the random occupation of the Si and Ge atoms on the B site altering the bond environments. A distribution of bond environments might result in a distribution of exchange constants broadening the Schottky-like specific-heat peak.

In magnetic fields, the peak in the specific heat is broadened and shifted to higher temperatures compared to zero field which is an expected behavior for this anomaly^{36,57,58}. The additional features that arise in field are also observed in Ref.³⁶ and may be attributed to the polycrystalline nature of the samples⁵⁸. Additional explanations are given in Ref.⁵⁹ by simulation methods. A definite conclusion could only be drawn with data obtained from single crystals.

The magnetic entropy was calculated from c_{mag}/T by integrating downwards from the temperature at which the curves with and without field overlap and fixing the plateaus at this value. The entropy data of $\text{Dy}_2\text{Ge}_2\text{O}_7$ and $\text{Dy}_2\text{Ge}_{1.875}\text{Si}_{0.125}\text{O}_7$ at zero field, 1, 2 and 4 T are compared in Fig. 7. The magnetic entropy of $\text{Dy}_2\text{Ge}_2\text{O}_7$ and $\text{Dy}_2\text{Ge}_{1.875}\text{Si}_{0.125}\text{O}_7$ shows a similar functional behavior. In external magnetic fields of 1 T and higher, the entropy of the ground state is recovered (Fig. 7). This behavior in an external field is typical for a spin-

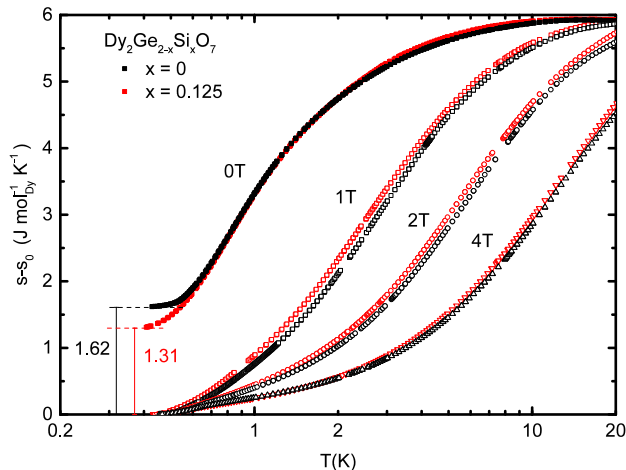


FIG. 7. Temperature dependence of the molar entropy of $\text{Dy}_2\text{Ge}_2\text{O}_7$ (black) and $\text{Dy}_2\text{Ge}_{1.875}\text{Si}_{0.125}\text{O}_7$ (red) at zero field (filled) and 1, 2 and 4 T (empty).

TABLE I. Lattice parameters and selected magnetic parameters to insert $\text{Dy}_2\text{Ge}_2\text{O}_7$ and $\text{Dy}_2\text{Ge}_{1.875}\text{Si}_{0.125}\text{O}_7$ in the phase diagram (Fig. 2).

x	a (Å)	D_{nn} (K)	$c_{\text{mag}}(T_{\text{peak}})$ ($\text{J mol}_{\text{Dy}}^{-1} \text{K}^{-1}$)	T_{peak} (K)	$J_{\text{nn}}/D_{\text{nn}}$	J_{eff} (K)
0	9.930	2.40	3.02	0.84	-0.71	0.69
0.125	9.906	2.42	3.07	0.80	-0.74	0.63

ice^{17,36,58} since the external magnetic field lifts the degeneracy of the ground state. The value of the ground-state entropy with $1.62 \text{ J mol}_{\text{Dy}}^{-1} \text{K}^{-1}$ (unsubstituted) and $1.31 \text{ J mol}_{\text{Dy}}^{-1} \text{K}^{-1}$ falls somewhat short of the Pauling entropy of $1.69 \text{ J mol}_{\text{Dy}}^{-1} \text{K}^{-1}$ of the ideal spin ice on a perfect crystal. The same arguments as for the peak height and width apply for this reduction, as well.

To place the new material in the phase diagram, we determined c_{mag} and T_{peak} from Fig. 6 and calculated the other values in Table I as explained in the following. We determined the dipolar interaction constant by the common estimation:

$$D_{\text{nn}} = \frac{5 \mu_0 g^2 \mu^2}{3 4\pi r_{\text{nn}}^3}, \quad (2)$$

with the moment assumed from the theoretical value of $g\mu = 10 \mu_{\text{B}}$ and $r_{\text{nn}} = \sqrt{2}a/4$ (a lattice constant) being the distance between two Dy^{3+} ions. Here we used the lattice constants determined at 300 K from the x-ray diffractograms to be consistent with other publications^{16,38}. Measurements of the thermal expansion of singlecrystalline samples of the isostructural compounds $\text{Dy}_2\text{Ti}_2\text{O}_7$ and $\text{Ho}_2\text{Ti}_2\text{O}_7$ down to low temperatures of about 1 K confirm that the assumed relations are largely retained. The reduction of the lattice constant of the Si-substituted sample, thus, leads to a slight increase of D_{nn} from 2.40 to 2.42 K. However, the increase

of the strength of the exchange interaction, J_{nn} , is more pronounced. Following the approach firstly described by den Hertog and Gingras¹² for $\text{Dy}_2\text{Ti}_2\text{O}_7$ and $\text{Ho}_2\text{Ti}_2\text{O}_7$ and used in several publications^{17,38} for Dy and Ho pyrochlores including $\text{Dy}_2\text{Ge}_2\text{O}_7$ and $\text{Ho}_2\text{Ge}_2\text{O}_7$, J_{nn} can be graphically determined on the $T_{\text{peak}}/D_{\text{nn}} - J_{\text{nn}}/D_{\text{nn}}$ line in the phase diagram (Fig. 2) as the intersection of the phase boundary between spin-ice and paramagnetic phase and the horizontal line with a specific ratio $T_{\text{peak}}/D_{\text{nn}}$. An increase of J_{nn} by 5% from $-1.70(5) \text{ K}$ to $-1.79(5) \text{ K}$ can be found. Therefore, the strength of the effective interaction $J_{\text{eff}} = D_{\text{nn}} + J_{\text{nn}}$ is reduced from $0.69(3) \text{ K}$ to $0.63(3) \text{ K}$ by about 10%. The reduction of the effective interaction is consistent with the reduced energy scale of the monopole excitation as seen in the ac susceptibility data (Fig. 5). We find that the activation energy $\Delta \approx -9J_{\text{eff}}$ agrees well with previous measurements on $\text{Dy}_2\text{Ti}_2\text{O}_7$ with $\Delta_{\text{Dy}_2\text{Ti}_2\text{O}_7} \approx -8.9J_{\text{eff}}$ ^{22,23}.

The value of J_{nn} can also be obtained from comparison of the value of specific-heat peak c_{peak} at the peak temperature with theoretical calculations¹². The experimental value of c_{peak} is around 10% lower than would be expected from theory for an ideal spin-ice with $J_{\text{nn}}/D_{\text{nn}} = -0.71$ or -0.74 obtained above, which might be due to crystal imperfections. However, it is consistent with the value of previous measurements of the peak height of $\text{Dy}_2\text{Ge}_2\text{O}_7$ ³⁸.

After careful consideration of Ref.³⁸, we come to the conclusion that the positioning of $\text{Dy}_2\text{Ge}_2\text{O}_7$ in the phase diagram (Table I) of that work is at the lower end of the possible region. While obtaining a similar value of T_{peak} they use a slightly higher value of D_{nn} . The fact that our $\text{Dy}_2\text{Ge}_{1.875}\text{Si}_{0.125}\text{O}_7$ sample has a lower $J_{\text{nn}}/D_{\text{nn}}$ than our $\text{Dy}_2\text{Ge}_2\text{O}_7$ as well as the sample investigated in Ref.³⁸ proves that the reduction of the effective interaction in this compound is significant.

From these data, three conclusions are drawn.

a. Spin-ice characteristics of $\text{Dy}_2\text{Ge}_{2-x}\text{Si}_x\text{O}_7$: The XRD data show the high quality of the materials and confirm the pyrochlore structure with the Dy^{3+} ions at the A site and randomly distributed Ge and Si at the B site. The magnetization data are close to the expected curve of the powder-averaged paramagnetic Ising spins providing evidence for the Ising nature of the moments of the Dy^{3+} ions due to the strong crystal electric field also observed in other spin-ice pyrochlores⁶⁰. The shape of the temperature-dependent ac susceptibility of Si-substituted Dy germanate resembles the ac susceptibility of the base compound and the well-studied spin-ice materials $\text{Dy}_2\text{Ti}_2\text{O}_7$ ¹⁹ and $\text{Dy}_2\text{Sn}_2\text{O}_7$ ⁶¹. However, a substantial difference in the frequency dependence could be identified, which originates in a reduction of τ_0 . The specific heats of $\text{Dy}_2\text{Ge}_2\text{O}_7$ and $\text{Dy}_2\text{Ge}_{1.875}\text{Si}_{0.125}\text{O}_7$ have a similar shape at low temperatures also in accordance with previous measurements of the specific heat of the classical spin ices $\text{Dy}_2\text{Ti}_2\text{O}_7$ ³⁴ and $\text{Ho}_2\text{Ti}_2\text{O}_7$ ³⁵. Another evidence for $\text{Dy}_2\text{Ge}_{1.875}\text{Si}_{0.125}\text{O}_7$ having spin-ice character is the residual entropy we observed. However, the resid-

ual entropy of $\text{Dy}_2\text{Ge}_{1.875}\text{Si}_{0.125}\text{O}_7$ is reduced compared to the Pauling entropy of the ideal spin-ice, possibly a side effect of the random distribution of Si and Ge on the B site of the pyrochlore lattice. In conclusion, the $\text{Dy}_2\text{Ge}_2\text{O}_7$ and $\text{Dy}_2\text{Ge}_{1.875}\text{Si}_{0.125}\text{O}_7$ samples, representing $\text{Dy}_2\text{Ge}_{2-x}\text{Si}_x\text{O}_7$, share several characteristic properties that are common among spin-ice materials.

b. Reduction of the effective nearest-neighbor interaction by 10%: Zhou *et al.*³⁸ have found that substituting ions with smaller ionic radius on the B site of the Dy-pyrochlores $\text{Dy}_2\text{Sn}_2\text{O}_7$ and $\text{Dy}_2\text{Ti}_2\text{O}_7$ reduces the peak temperature of the magnetic specific heat. The authors linked this to a reduction of the effective interaction due to the reduction of the distance between neighboring Dy^{3+} ions using the $T_{\text{peak}}/D_{\text{nn}}-J_{\text{nn}}/D_{\text{nn}}$ phase diagram of the dipolar-spin-ice model¹². Our XRD measurements confirm the reduced lattice constants in $\text{Dy}_2\text{Ge}_2\text{O}_7$ compared to $\text{Dy}_2\text{Ti}_2\text{O}_7$ ³⁸. The Si-substituted samples continue this trend towards a reduction of the lattice constants and the peak temperatures in the specific heat as well as in the ac susceptibility. Therefore, we argue, that in $\text{Dy}_2\text{Ge}_{2-x}\text{Si}_x\text{O}_7$ the competing dipolar and exchange interactions are even further increased compared to $\text{Dy}_2\text{Ge}_2\text{O}_7$. Since the increase of the exchange interaction is stronger than the increase of the dipolar interaction, the total effective interaction is reduced compared to $\text{Dy}_2\text{Ge}_2\text{O}_7$.

c. Influence of disorder on the spin-ice character A thorough study of the effects of disorder on the B site of the spin-ice pyrochlores is not possible with the samples in this paper. But still, the currently highly discussed influence of a stoichiometric or crystallographic disorder can be considered. It is known⁶²⁻⁶⁴ that strong modification of the regular structure can lead to the elimination of frustration, the formation of magnetically ordered clusters or the loss of the Ising character in pyrochlore compounds. Quantum fluctuations can then have an increased effect and weaken the spin-ice character. Although the distribution in the Ge/Si system is random (could be checked by synchrotrons), the low Si content does not seem to be sufficient to eliminate the magnetic frustration in the Dy sublattice. Averaging over microscopically different areas mostly recovers the spin-ice properties of the system.

IV. SUMMARY

High-quality polycrystals of the pyrochlores $\text{Dy}_2\text{Ge}_{2-x}\text{Si}_x\text{O}_7$ with lattice constants down to 9.906 Å using the multi-anvil technique with pressures up to 16 GPa have been synthesized. The Ising nature of the moments of the Dy ions was confirmed by the field dependence of the static magnetization. Specific heat and ac susceptibility show the typical behavior of classical spin-ice compounds, namely a Schottky-like anomaly and residual entropy, and a frequency-dependent maximum, respectively. The reduction of the lattice constant increases both the dipolar as well as the exchange-interaction strength. However, while the dipolar interaction is only increased by less than 1%, the exchange interaction increases by 5%, leading to a reduction of the effective interaction by 10%. Consequently, the silicon-substituted sample is closer to the phase boundary between the short-range spin-ice arrangement and the long-range AFM order. The most significant difference between the substituted and unsubstituted compounds was found in the frequency dependence of the ac-susceptibility signal, which mainly originates in a reduction of the pre-exponential factor τ_0 . However, a reduction of the energy scale of monopole excitations of 1.5% was observed as well, which underlines the finding of a reduced effective interaction. In conclusion, we showed, that silicon substitution is a possible way to change the ratio of dipolar and exchange interaction and, hence, synthesize spin-ice compounds with customized properties. The further increase of the substitutions on the B site of the pyrochlores with improved high-pressure synthesis technology could open the possibility to study how disorder on the B site of the pyrochlore influences the (spin-ice) characteristics⁶², e.g. through the formation of pinning centers, in view of work on other disordered materials⁶⁵⁻⁶⁷. Furthermore, the growth and investigation of single crystals of $\text{Dy}_2\text{Ge}_2\text{O}_7$ and its silicon-substituted compounds can be a challenging future task and offer the possibility to characterize the samples in terms of more recent spin-ice models including exchange interactions beyond nearest neighbors^{42,44,45}.

ACKNOWLEDGMENTS

We acknowledge support for using the ALBA synchrotron light source in Barcelona, Spain, and from HLD at HZDR, member of the European Magnetic Field Laboratory (EMFL). This research has been supported by the DFG through SFB 1143 (project-id 247310070).

¹ J. E. Greedan, *J. Mater. Chem.* **11**, 37 (2001).

² J. E. Greedan, *J. Alloys Compd.* **408-412**, 444 (2006).

³ A. P. Ramirez, *Annu. Rev. Mater. Sci.* **24**, 453 (1994).

- ⁴ J. Wosnitza, S. A. Zvyagin, and S. Zherlitsyn, Rep. Prog. Phys. **79**, 074504 (2016).
- ⁵ L. Balents, Nature **464**, 199 (2010).
- ⁶ M. J. P. Gingras and P. A. McClarty, Rep. Prog. Phys. **77**, 056501 (2014).
- ⁷ A. A. Zvyagin, Low Temp. Phys. **39**, 901 (2013).
- ⁸ J. S. Gardner, M. J. P. Gingras, and J. E. Greedan, Rev. Mod. Phys. **82**, 53 (2010).
- ⁹ J. G. Rau and M. J. P. Gingras, Annu. Rev. Condens. Matter Phys. **10**, 357 (2019).
- ¹⁰ S. Rosenkranz, A. P. Ramirez, A. Hayashi, R. J. Cava, R. Siddharthan, and B. S. Shastry, J. Appl. Phys. **87**, 5914 (2000).
- ¹¹ J. G. Rau and M. J. P. Gingras, Phys. Rev. B **92**, 144417 (2015).
- ¹² B. C. den Hertog and M. J. P. Gingras, Phys. Rev. Lett. **84**, 3430 (2000).
- ¹³ A. Bertin, P. Dalmas de Réotier, B. Fåk, C. Marin, A. Yaouanc, A. Forget, D. Sheptyakov, B. Frick, C. Ritter, A. Amato, C. Baines, and P. J. C. King, Phys. Rev. B **92**, 144423 (2015).
- ¹⁴ L. Opherden, J. Hornung, T. Herrmannsdörfer, J. Xu, A. T. M. N. Islam, B. Lake, and J. Wosnitza, Phys. Rev. B **95**, 184418 (2017).
- ¹⁵ L. Opherden, T. Bilitewski, J. Hornung, T. Herrmannsdörfer, A. Samartzis, A. T. M. N. Islam, V. K. Anand, B. Lake, R. Moessner, and J. Wosnitza, Phys. Rev. B **98**, 180403(R) (2018).
- ¹⁶ J. Xu, V. K. Anand, A. K. Bera, M. Frontzek, D. L. Abernathy, N. Casati, K. Siemensmeyer, and B. Lake, Phys. Rev. B **92**, 224430 (2015).
- ¹⁷ S. T. Bramwell and M. J. P. Gingras, Science **294**, 1495 (2001).
- ¹⁸ C. Castelnovo, R. Moessner, and S. L. Sondhi, Nature **451**, 42 (2008).
- ¹⁹ K. Matsuhira, Y. Hinatsu, and T. Sakakibara, J. Phys. Condens. Matter **13**, L737 (2001).
- ²⁰ J. Snyder, B. G. Ueland, J. S. Slusky, H. Karunadasa, R. J. Cava, A. Mizel, and P. Schiffer, Phys. Rev. Lett. **91**, 107201 (2003).
- ²¹ J. Snyder, B. G. Ueland, J. S. Slusky, H. Karunadasa, R. J. Cava, and P. Schiffer, Phys. Rev. B **69**, 064414 (2004).
- ²² K. Matsuhira, C. Paulsen, E. Lhotel, C. Sekine, Z. Hiroi, and S. Takagi, J. Phys. Soc. Jpn. **80**, 123711 (2011).
- ²³ L. R. Yaraskavitch, H. M. Revell, S. Meng, K. A. Ross, H. M. L. Noad, H. A. Dabkowska, B. D. Gaulin, and J. B. Kycia, Phys. Rev. B **85**, 020410(R) (2012).
- ²⁴ K. Matsuhira, Y. Hinatsu, K. Tenya, and T. Sakakibara, J. Phys. Condens. Matter **12**, L649 (2000).
- ²⁵ J. Snyder, J. S. Slusky, R. J. Cava, and P. Schiffer, Nature **413**, 48 (2001).
- ²⁶ G. Ehlers, A. L. Cornelius, M. Orendác, M. Kajnaková, T. Fennell, S. T. Bramwell, and J. S. Gardner, J. Phys. Condens. Matter **15**, L9 (2003).
- ²⁷ G. Ehlers, A. L. Cornelius, T. Fennell, M. Koza, S. T. Bramwell, and J. S. Gardner, J. Phys. Condens. Matter **16**, S635 (2004).
- ²⁸ J. A. Quilliam, L. R. Yaraskavitch, H. A. Dabkowska, B. D. Gaulin, and J. B. Kycia, Phys. Rev. B **83**, 094424 (2011).
- ²⁹ L. D. C. Jaubert and P. C. W. Holdsworth, J. Phys. Condens. Matter **23**, 164222 (2011).
- ³⁰ T. Sakakibara, T. Tayama, Z. Hiroi, K. Matsuhira, and S. Takagi, Phys. Rev. Lett. **90**, 207205 (2003).
- ³¹ C. Krey, S. Legl, S. R. Dunsiger, M. Meven, J. S. Gardner, J. M. Roper, and C. Pfleiderer, Phys. Rev. Lett. **108**, 257204 (2012).
- ³² O. A. Petrenko, M. R. Lees, and G. Balakrishnan, Phys. Rev. B **68**, 012406 (2003).
- ³³ Z. Hiroi, K. Matsuhira, S. Takagi, T. Tayama, and T. Sakakibara, J. Phys. Soc. Jpn. **72**, 411 (2003).
- ³⁴ R. Higashinaka, H. Fukazawa, K. Deguchi, and Y. Maeno, J. Phys. Soc. Jpn. **73**, 2845 (2004).
- ³⁵ S. T. Bramwell, M. J. Harris, B. C. den Hertog, M. J. P. Gingras, J. S. Gardner, D. F. McMorrow, A. R. Wildes, A. L. Cornelius, J. D. M. Champion, R. G. Melko, and T. Fennell, Phys. Rev. Lett. **87**, 047205 (2001).
- ³⁶ A. P. Ramirez, A. Hayashi, R. J. Cava, R. Siddharthan, and B. S. Shastry, Nature **399**, 333 (1999).
- ³⁷ S. R. Giblin, M. Twengström, L. Bovo, M. Ruminy, M. Bartkowiak, P. Manuel, J. C. Andresen, D. Prabhakaran, G. Balakrishnan, E. Pomjakushina, C. Paulsen, E. Lhotel, L. Keller, M. Frontzek, S. C. Capelli, O. Zaharko, P. A. McClarty, S. T. Bramwell, P. Henelius, and T. Fennell, Phys. Rev. Lett. **121**, 067202 (2018).
- ³⁸ H. D. Zhou, J. G. Cheng, A. M. Hallas, C. R. Wiebe, G. Li, L. Balicas, J. S. Zhou, J. B. Goodenough, J. S. Gardner, and E. S. Choi, Phys. Rev. Lett. **108**, 207206 (2012).
- ³⁹ D. Pomaranski, L. R. Yaraskavitch, S. Meng, K. A. Ross, H. M. L. Noad, H. A. Dabkowska, B. D. Gaulin, and J. B. Kycia, Nat. Phys. **9**, 353 (2013).
- ⁴⁰ R. G. Melko, B. C. den Hertog, and M. J. P. Gingras, Phys. Rev. Lett. **87**, 067203 (2001).
- ⁴¹ R. G. Melko and M. J. P. Gingras, J. Phys. Condens. Matter **16**, R1277 (2004).
- ⁴² P. A. McClarty, O. Sikora, R. Moessner, K. Penc, F. Pollmann, and N. Shannon, Phys. Rev. B **92**, 094418 (2015).
- ⁴³ T. Yavors'kii, T. Fennell, M. J. P. Gingras, and S. T. Bramwell, Phys. Rev. Lett. **101**, 037204 (2008).
- ⁴⁴ P. Henelius, T. Lin, M. Enjalran, Z. Hao, J. G. Rau, J. Altonsoar, F. Flicker, T. Yavors'kii, and M. J. P. Gingras, Phys. Rev. B **93**, 024402 (2016).
- ⁴⁵ J. G. Rau and M. J. P. Gingras, Nat. Commun. **7**, 12234 (2016).
- ⁴⁶ H. D. Zhou, S. T. Bramwell, J. G. Cheng, C. R. Wiebe, G. Li, L. Balicas, J. A. Bloxson, H. J. Silverstein, J. S. Zhou, J. B. Goodenough, and J. S. Gardner, Nat. Commun. **2**, 478 (2011).
- ⁴⁷ C. R. Wiebe and A. M. Hallas, APL Mater. **3**, 041519 (2015).
- ⁴⁸ I. Mirebeau and I. Goncharenko, J. Phys. Condens. Matter **16**, S653 (2004).
- ⁴⁹ R. Mouta, R. X. Silva, and C. W. A. Paschoal, Acta Crystallogr. Sec. B **69**, 439 (2013).
- ⁵⁰ R. D. Shannon and C. T. Prewitt, Acta Crystallogr. Sec. B **25**, 925 (1969).
- ⁵¹ D. Walker, M. A. Carpenter, and C. M. Hitch, Am. Mineral. **75**, 1020 (1990).
- ⁵² T. H. K. Barron and G. K. White, *Heat Capacity and Thermal Expansion at Low Temperatures* (Springer US, Boston, MA, 1999).
- ⁵³ S. T. Bramwell, M. N. Field, M. J. Harris, and I. P. Parkin, J. Phys. Condens. Matter **12**, 483 (2000).
- ⁵⁴ B. Tomasello, C. Castelnovo, R. Moessner, and J. Quintanilla, arXiv e-prints, arXiv:1810.11469 (2018).
- ⁵⁵ K. Matsuhira, M. Wakeshima, Y. Hinatsu, C. Sekine, C. Paulsen, T. Sakakibara, and S. Takagi, J. Phys. Conf. Ser. **320**, 012050 (2011).

- ⁵⁶ S. Gao, O. Zaharko, V. Tsurkan, L. Prodan, E. Riordan, J. Lago, B. Fåk, A. R. Wildes, M. M. Koza, C. Ritter, P. Fouquet, L. Keller, E. Canévet, M. Medarde, J. Blomgren, C. Johansson, S. R. Giblin, S. Vrtnik, J. Luzar, A. Loidl, C. Rüegg, and T. Fennell, *Phys. Rev. Lett.* **120**, 137201 (2018).
- ⁵⁷ S.-Y. Kim, *J. Kor. Phys. Soc.* **65**, 970 (2014).
- ⁵⁸ R. Higashinaka, H. Fukazawa, D. Yanagishima, and Y. Maeno, *J. Phys. Chem. Solid* **63**, 1043 (2002).
- ⁵⁹ J. P. C. Ruff, R. G. Melko, and M. J. P. Gingras, *Phys. Rev. Lett.* **95**, 097202 (2005).
- ⁶⁰ A. Bertin, Y. Chapuis, P. Dalmas de Réotier, and A. Yaouanc, *J. Phys. Condens. Matter* **24**, 256003 (2012).
- ⁶¹ K. Matsuhira, Y. Hinatsu, K. Tenya, H. Amitsuka, and T. Sakakibara, *J. Phys. Soc. Jpn.* **71**, 1576 (2002).
- ⁶² L. Savary and L. Balents, *Phys. Rev. Lett.* **118**, 087203 (2017).
- ⁶³ N. Martin, P. Bonville, E. Lhotel, S. Guitteny, A. Wildes, C. Decorse, M. Ciomaga Hatnean, G. Balakrishnan, I. Mirebeau, and S. Petit, *Phys. Rev. X* **7**, 041028 (2017).
- ⁶⁴ J.-J. Wen, S. M. Koohpayeh, K. A. Ross, B. A. Trump, T. M. McQueen, K. Kimura, S. Nakatsuji, Y. Qiu, D. M. Pajerowski, J. R. D. Copley, and C. L. Broholm, *Phys. Rev. Lett.* **118**, 107206 (2017).
- ⁶⁵ Y. Li, D. Adroja, R. I. Bewley, D. Voneshen, A. A. Tsirlin, P. Gegenwart, and Q. Zhang, *Phys. Rev. Lett.* **118**, 107202 (2017).
- ⁶⁶ Z. Zhu, P. A. Maksimov, S. R. White, and A. L. Chernyshev, *Phys. Rev. Lett.* **119**, 157201 (2017).
- ⁶⁷ G. Sala, M. J. Gutmann, D. Prabhakaran, D. Pomaranski, C. Mitchelitis, J. B. Kycia, D. G. Porter, C. Castelnovo, and J. P. Goff, *Nat. Mater.* **13**, 488 (2014).